Journal of Solid State Chemistry **142,** 33–40 (1999)
Article ID jssc.1998.7980, available online at http://www.idealibrary.com on IDEAL®

Modeling and Rietveld-Refinement of the Crystal Structure of $Bi_4Ta_2O_{11}$ Based on That of $Bi_7Ta_3O_{18}$

Christopher D. Ling,[1] John G. Thompson, Ray L. Withers, and Siegbert Schmid

Research School of Chemistry, Australian National University, Canberra, ACT 0200, Australia

Received March 10, 1998, in revised form July 20, 1998; accepted July 27, 1998

A $P\bar{1}$ model for the crystal structure of $Bi_4Ta_2O_{11}$ has been proposed based on units from the $P1$ crystal structure of $Bi_7Ta_3O_{38}$. The model was found to be plausible in terms of bond valence sums. When refined via the Rietveld method using X-ray (synchrotron) and neutron powder diffraction data, the final structure had greatly improved bond valence sums. The metal atom array approximates fluorite-type with regular "step" defects on $(h\,k\,0)$ planes (perpendicular to $[1\,1\,1]_{\text{fluorite}}$). Regular TaO_6 octahedra form corner-connected columns. Bismuth atoms are in high coordination environments similar to those found in fluorite-type. $Bi_7Ta_3O_{18}$ and $Bi_4Ta_2O_{11}$ are discussed in terms of their structural relationships to one another, to adjacent phases in the Bi_2O_3–Ta_2O_5 system, and to structures proposed by earlier authors based on an archetypal fluorite-type substructure.

INTRODUCTION

The high-temperature form of bismuth oxide, δ-Bi_2O_3, is one of the best oxygen ion conductors known (1, 2). It is reported as a face-centred-cubic (fcc), fluorite-type structure, with 25% average oxygen vacancies accounting for its anionic conduction properties (3, 4). The δ-Bi_2O_3 structure cannot be quenched to room temperature; however, its fluorite-related structure and ionic conduction properties are approximately preserved at room temperature in some bismuth-rich phases in binary oxide systems involving certain transition metal oxides (5, 6). These phases appear to have modulated structures based on an underlying fluorite-related substructure.

We recently reinvestigated bismuth-rich phases in a number of binary oxide systems (7), including Bi_2O_3–Ta_2O_5. This system was investigated in an X-ray powder diffraction (XRD) study by Levin and Roth (8), and more recently in a transmission electron microscopy (TEM) study by Zhou (9), who reported the new phases $Bi_7Ta_3O_{18}$ and $Bi_4Ta_2O_{11}$as commensurately modulated δ-Bi_2O_3-related superstructure types II* and III, respectively. We reproduced the electron diffraction patterns reported for $Bi_7Ta_3O_{18}$ and $Bi_4Ta_2O_{11}$ but in both cases derived unit cells apparently unrelated to those reported by Zhou (9). There were no unambiguous fluorite-type subcells, despite observation of ostensibly fluorite-like projections of the reciprocal sublattices. The strongest reflections present in synchrotron XRD data also could not be unambiguously indexed as fluorite. It was concluded that while $Bi_7Ta_3O_{18}$ and $Bi_4Ta_2O_{11}$ might incorporate structural elements of δ-Bi_2O_3, they must be too far removed from that prototype to be usefully described as modulated variants thereof.

We have recently solved the crystal structure of $Bi_7Ta_3O_{18}$ using single-crystal X-ray and powder neutron diffraction data (10). The relationship of that structure to fluorite is found in the metal atom array, which is based on displacement faulted slabs of fluorite-type, hence the ambiguity of fluorite-type subcells in the average reciprocal lattice. Metal populations are fully ordered. Oxygen atoms bonded to tantalum atoms deviate significantly from fluorite in order to create octahedral coordination environments. Bismuth atoms are in high coordination environments amid columns of corner-connected TaO_6 octahedra, with the remaining oxygen atoms occupying distorted fluorite positions.

Strong similarities between the unit cells and electron diffraction patterns of $Bi_7Ta_3O_{18}$ and $Bi_4Ta_2O_{11}$ indicated structural similarities between the two phases. The present study sets out to develop a model for the structure of $Bi_4Ta_2O_{11}$ based on the structure of $Bi_7Ta_3O_{18}$, to test it quantitatively using synchrotron XRD and powder neutron diffraction data, and thereby to come to an understanding of the structural principles underlying this type of structure.

SYNTHESES

A powder sample of $Bi_4Ta_2O_{11}$ was prepared by solid-state reaction of a mixture of Bi_2O_3 (Koch-Lite 99.998%) and Ta_2O_5 (Aldrich 99.99%) at mole ratio 2:1 in a platinum crucible at 1103 K for 0.5 h. The sample was quenched to

[1]To whom correspondence should be addressed.

0022-4596/99 $30.00

room temperature, reground, annealed in a sealed platinum vessel at 1173 K for 192 h, and again quenched to room temperature. A homogeneous, pale yellow powder was obtained and identified as single-phase $Bi_4Ta_2O_{11}$ by XRD (Jungner XDC-700 Guinier-Hägg camera) (7).

Synchrotron XRD data were collected at Beam Line 20B at the Photon Factory in Tsukuba, Japan. The pattern was collected across three image plates at a wavelength of 1.4986 Å, from $2\theta = 5$ to 125°. Si (NBS 640) was used as an internal standard.

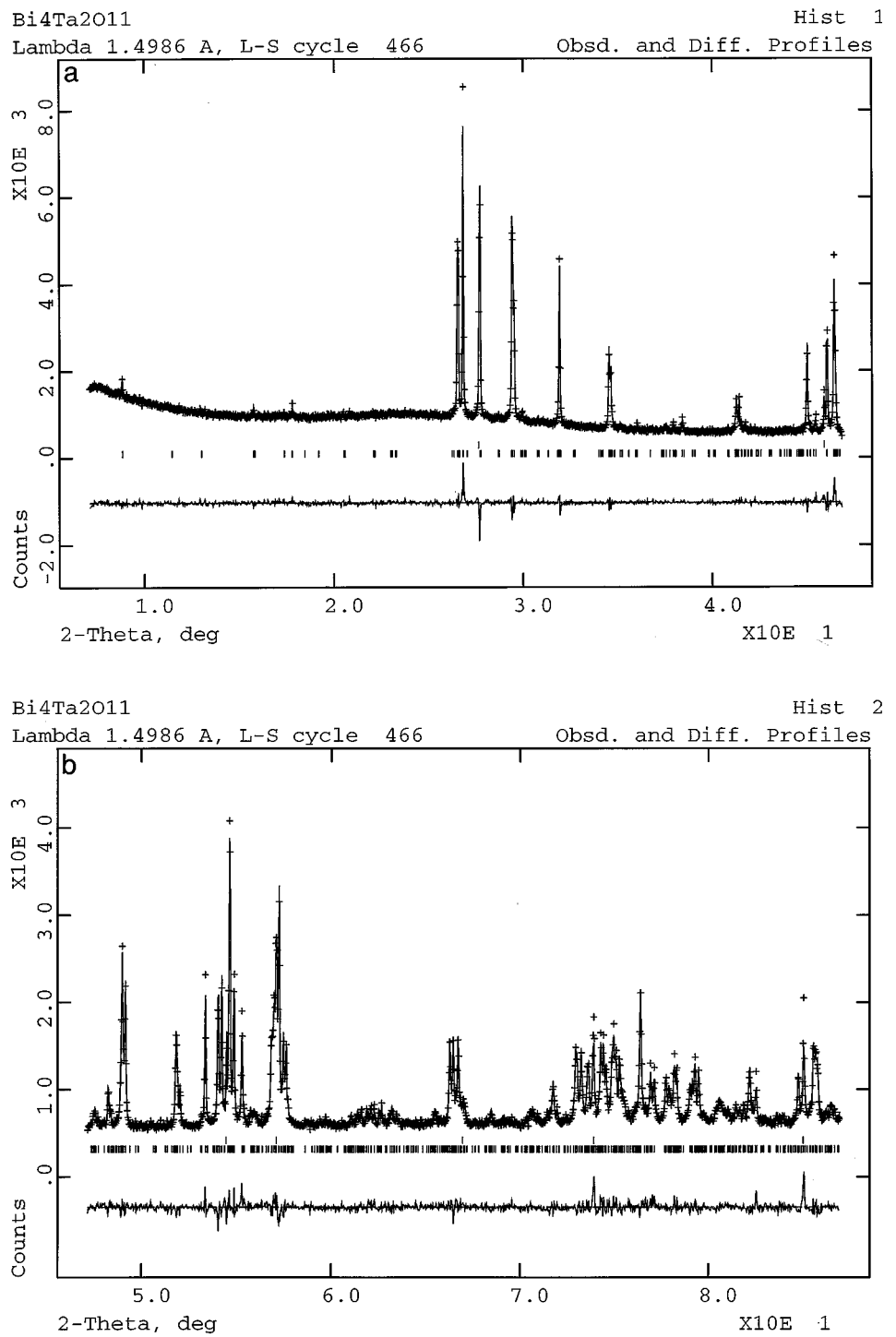

FIG. 1. Observed (+), calculated, and difference (bottom) XRD profiles for $Bi_4Ta_2O_{11}$ from (a) 5–45°, (b) 45–85°, and (c) 85–125° 2θ. The top row of reflection markers refers to the Si standard.

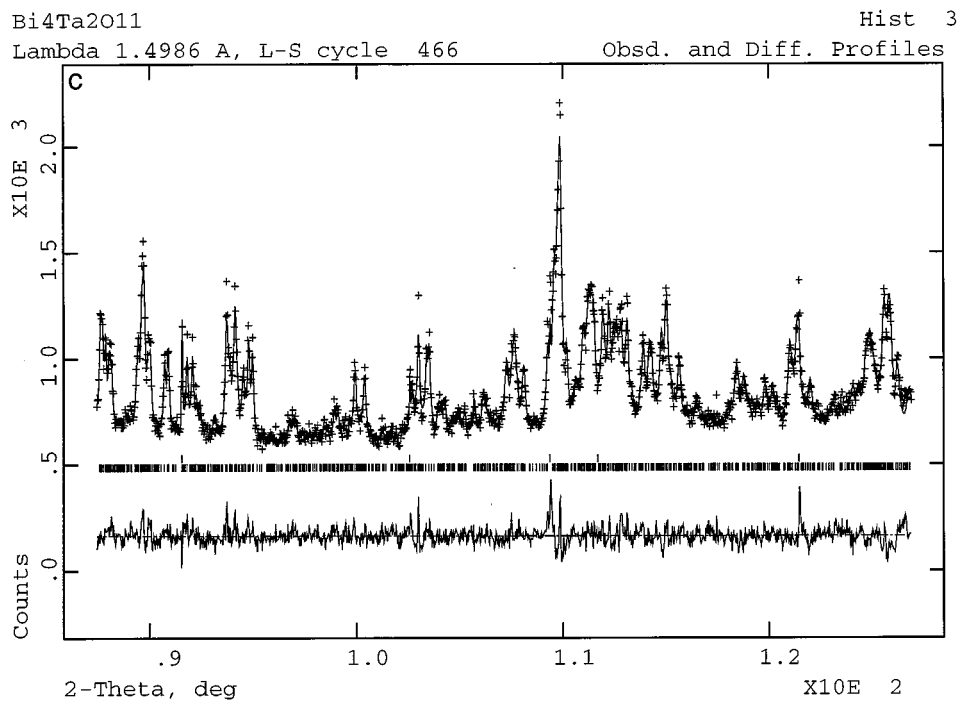

FIG. 1—*Continued*

Powder neutron diffraction data were collected on POLARIS (11), the high flux, medium resolution time-of-flight instrument at ISIS (Rutherford Appleton Laboratories, UK). The high flux of POLARIS was sought due to difficulties encountered in obtaining a large, homogenous sample via the method described above. Patterns were collected on the A (35°), C (145°), and E (90°) detector banks (11).

MODELING

The first consideration in proposing a model for the structure of $Bi_4Ta_2O_{11}$ was the relationship of its unit cell to that of $Bi_7Ta_3O_{18}$. The reduced, primitive cells determined from XRD (7) are compared in Table 1.

The most significant difference between the two cells was clearly the length of the long c-axis. $Bi_7Ta_3O_{18}$ is essentially composed of five layers of metal atoms layered perpendicular to c(10). Given that $c(Bi_4Ta_2O_{11}) \approx \frac{3}{5}c(Bi_7Ta_3O_{18})$, it seemed very likely that $Bi_4Ta_2O_{11}$ was composed of three layers in the same manner.

The second consideration in proposing a model was the compositions of the respective phases. The average populations of the five metal atom layers in $Bi_7Ta_3O_{18}$ follow the sequence $Bi_{1/2}Ta_{1/2}$–Bi–$Bi_{1/2}Ta_{1/2}$–Bi–$Bi_{1/2}Ta_{1/2}$. The only way to change the overall composition to $Bi_4Ta_2O_{11}$ while maintaining the same interlayer connectivity was to collapse this sequence to $Bi_{1/2}Ta_{1/2}$–Bi–$Bi_{1/2}Ta_{1/2}$.

The final aspect of the model to be considered was the possible presence of symmetry elements not previously

TABLE 1
Comparison of the Unit Cells of $Bi_7Ta_3O_{18}$ and $Bi_4Ta_2O_{11}$

	$Bi_7Ta_3O_{18}$	$Bi_4Ta_2O_{11}$
a (Å)	6.6358(7)	6.6112(7)
b (Å)	7.6024(8)	7.6607(8)
c (Å)	16.5364(17)	9.8899(10)
α (°)	103.208(10)	101.280(10)
β (°)	93.672(9)	90.201(9)
γ (°)	90.086(9)	90.020(9)

TABLE 2
Rietveld Refinement Statistics for $Bi_4Ta_2O_{11}$

	R_p	wR_p	$R(F^2)$	χ^2
X-rays				
5–45° 2θ	0.0296	0.0407	0.0841	
45–85° 2θ	0.0358	0.0474	0.0681	
85–125° 2θ	0.0339	0.0440	0.0539	
Overall	0.0328	0.0439		1.691
Neutrons				
35° 2θ	0.0414	0.0406	0.0267	
90° 2θ	0.0448	0.0379	0.0288	
145° 2θ	0.0604	0.0391	0.0210	
Overall	0.0487	0.0388		16.16

determinable by systematically absent diffraction peaks. It was found that the presence of any mirror plane or rotation axis was incompatible with maintenance of the interlayer connectivity found in $Bi_7Ta_3O_{18}$. The presence of an inversion center did not, however, disrupt this connectivity and was therefore incorporated into the initial model ($P\bar{1}$) in order to reduce the number of refined variables. Note that there is no inversion centre in the refined structure of $Bi_7Ta_3O_{18}$ ($P1$). For further consideration of the symmetry of these phases see the Discussion below.

Fractional atomic coordinates for $Bi_4Ta_2O_{11}$ were obtained from those of the final refined structure of $Bi_7Ta_3O_{18}$

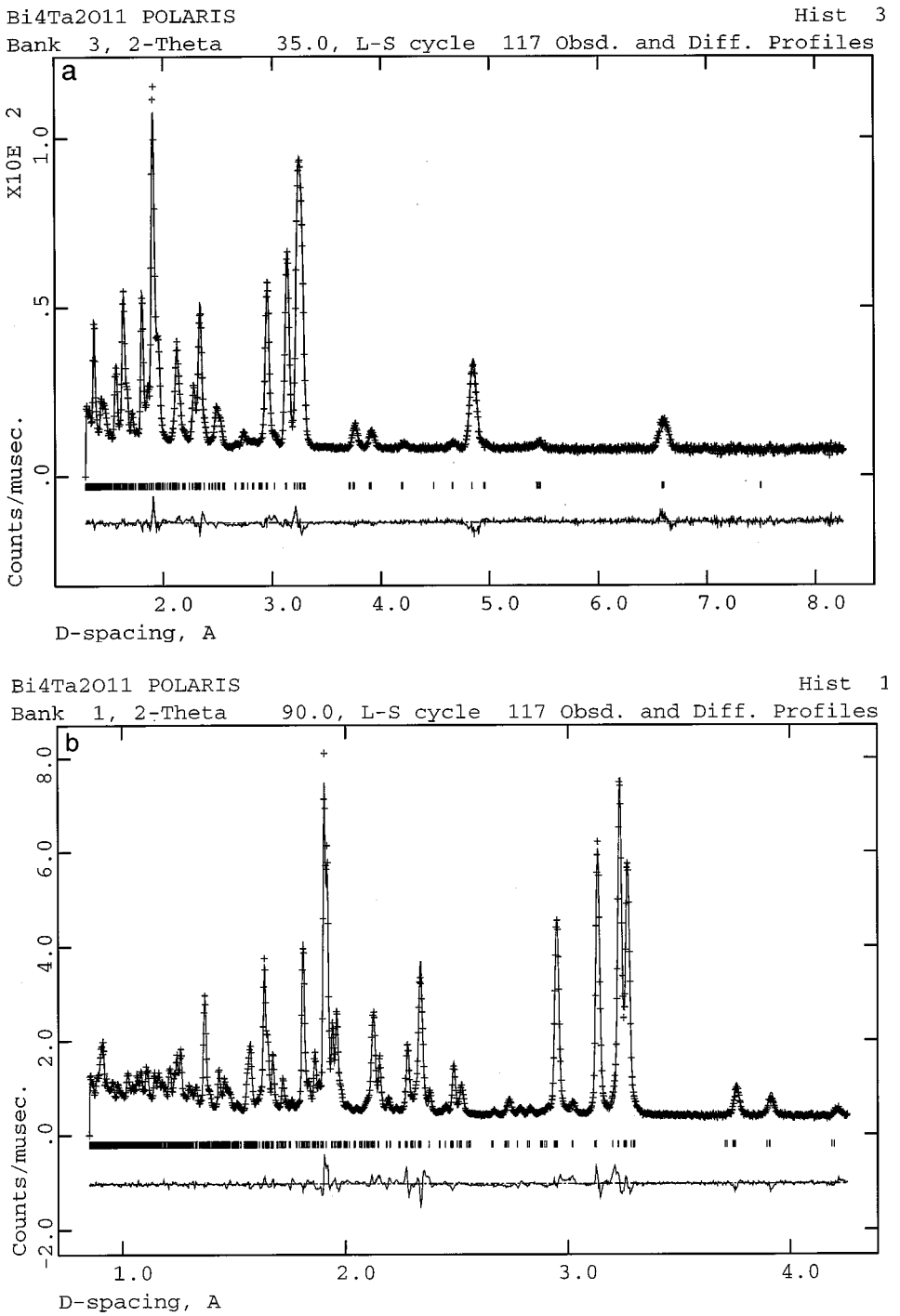

FIG. 2. Observed (+), calculated, and difference (bottom) neutron powder diffraction profiles for $Bi_4Ta_2O_{11}$ at the (a) 35°, (b) 90° and (c) 145° detector banks (11).

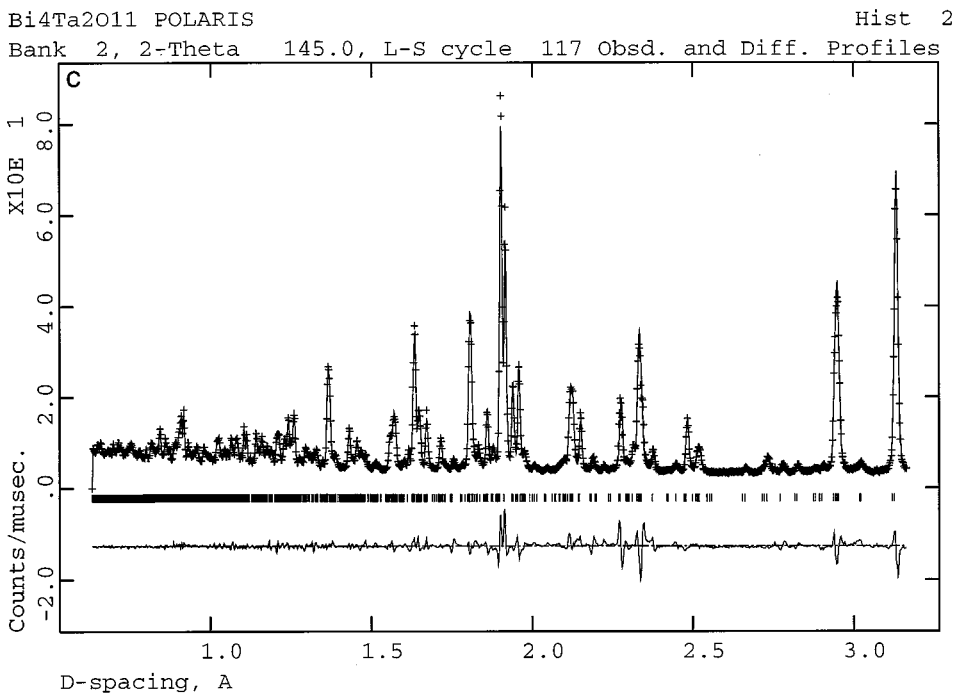

FIG. 2—*Continued*

(10) by selecting atoms from the first two layers and introducing an inversion center. Atoms in the middle layer had their coordinates averaged about the inversion centre. Fractional z coordinates were multiplied by 5/3 to account for the shorter cell of $Bi_4Ta_2O_{11}$.

REFINEMENT

The relatively small contribution of oxygen atoms to the X-ray scattering of $Bi_4Ta_2O_{11}$ allowed unconstrained refinement of metal atom parameters (positional and isotropic displacement) from the initial model while fixing the oxygen

TABLE 3
Final Refined Fractional Coordinates and U_{iso} Values for $Bi_4Ta_2O_{11}$

Atom	x	y	z	$100U_{iso}$
Bi(1)	0.6057(4)	0.5414(6)	0.1665(3)	0.236(15)
Bi(2)	0.5713(4)	0.0448(5)	0.1808(3)	0.236(15)
Bi(3)	0.2499(4)	0.1328(5)	0.5225(3)	0.236(15)
Bi(4)	0.2386(4)	0.6388(5)	0.5139(3)	0.236(15)
Ta(1)	0.0902(5)	0.7955(7)	0.1911(4)	0.236(15)
Ta(2)	0.0850(6)	0.2929(7)	0.1875(4)	0.236(15)
O(1)	0.0234(5)	0.5476(11)	0.1858(4)	0.90(2)
O(2)	0.9973(10)	0.7795(5)	0.9999(7)	0.90(2)
O(3)	0.5933(7)	0.6166(7)	0.3789(5)	0.90(2)
O(4)	0.1597(6)	0.0533(10)	0.2132(4)	0.90(2)
O(5)	0.5416(6)	0.0976(9)	0.3949(4)	0.90(2)
O(6)	0.0911(7)	0.3713(8)	0.4013(5)	0.90(2)
O(7)	0.7836(8)	0.8546(7)	0.2409(6)	0.90(2)
O(8)	0.1100(7)	0.8264(7)	0.3957(5)	0.90(2)
O(9)	0.3751(8)	0.7468(8)	0.1576(5)	0.90(2)
O(10)	0.3752(9)	0.3468(7)	0.1692(6)	0.90(2)
O(11)	0.7843(8)	0.2682(6)	0.2326(5)	0.90(2)

TABLE 4
Bond Valence Sums (13) for the Initial and Final Refined Models of $Bi_4Ta_2O_{11}$

Atom	Initial	Refined	Expected
Bi(1)	3.031	3.353	3.000
Bi(2)	3.115	3.198	3.000
Bi(3)	4.573	3.038	3.000
Bi(4)	2.303	2.897	3.000
Ta(1)	5.107	5.000	5.000
Ta(2)	5.002	4.932	5.000
O(1)	1.891	1.922	2.000
O(2)	1.647	1.922	2.000
O(3)	2.405	2.190	2.000
O(4)	2.021	1.946	2.000
O(5)	2.277	2.265	2.000
O(6)	2.396	1.922	2.000
O(7)	2.135	2.117	2.000
O(8)	2.798	2.157	2.000
O(9)	1.873	1.952	2.000
O(10)	1.857	1.956	2.000
O(11)	1.832	2.068	2.000

atoms at their starting positions. Rietveld refinements were carried out using the program GSAS (12). The success of this initial refinement ($R_p = 0.0360$, $wR_p = 0.0549$, $\chi^2 = 2.703$) indicated that the metal atom array was essentially correct.

Oxygen atom parameters (positional and overall isotropic displacement) in this model were then refined using powder neutron diffraction data, converging rapidly ($R_p = 0.0543$, $wR_p = 0.0473$, $\chi^2 = 23.99$) and indicating that the oxygen atom array was also essentially correct.

Repeating the X-ray refinement of metal parameters using these refined oxygen parameters improved the result ($R_p = 0.0328$, $wR_p = 0.0439$, $\chi^2 = 1.691$). The observed, calculated, and difference XRD profiles at this stage are shown in Fig. 1. Note that the most significant features in the difference profiles correspond to diffraction peaks of the silicon standard, which were too weak (and too sharp) for adequate profile and phase fraction refinement. Refinement statistics for individual histograms are presented in Table 2.

Subsequently, unconstrained refinement of all positional parameters, as well as overall isotropic thermal displacement parameters for metal and oxygen atoms, using powder neutron diffraction data gave $R_p = 0.0487$, $wR_p = 0.0388$, and $\chi^2 = 16.16$. Refinement of independent isotropic displacement parameters for all atoms reduced this to $R_p = 0.0486$, $wR_p = 0.0381$, and $\chi^2 = 15.48$; however, this improvement in statistics was not considered significant given the number of new variables introduced. In addition,

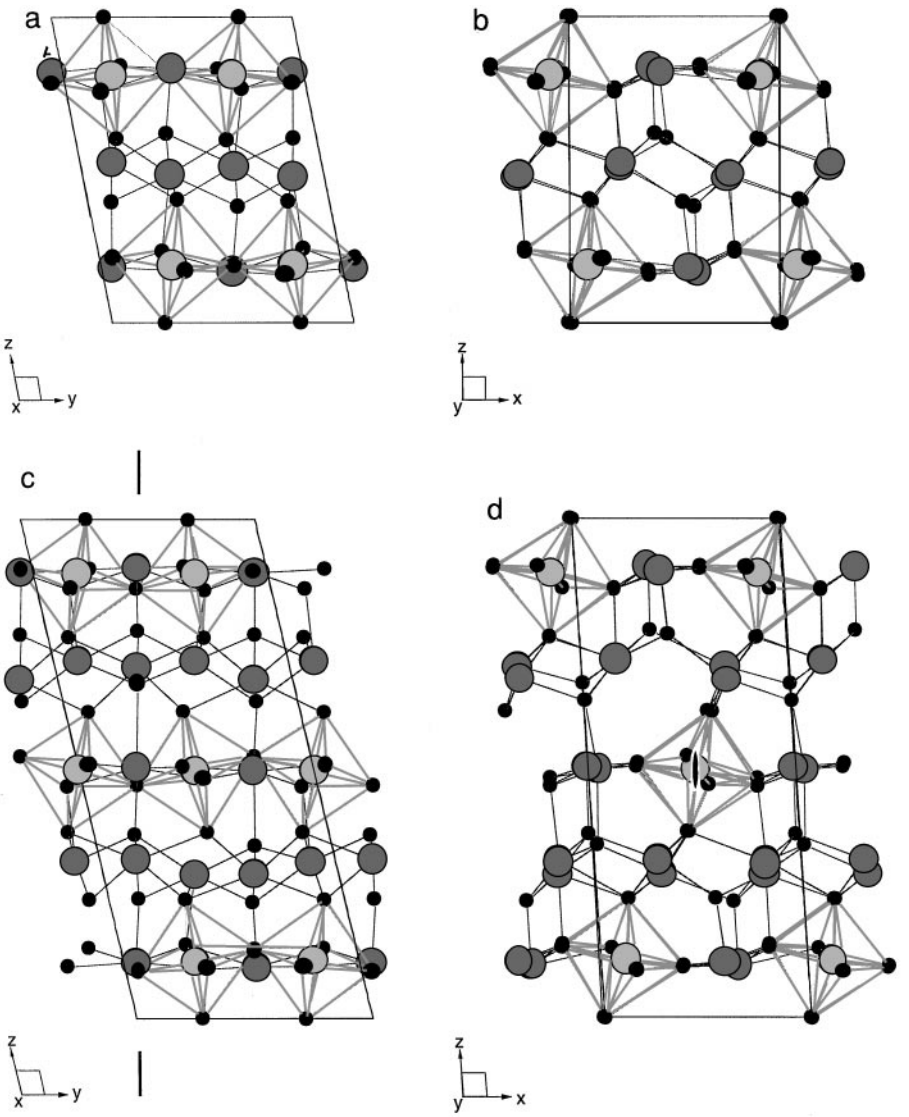

FIG. 3. The final refined $P\bar{1}$ structure of $Bi_4Ta_2O_{11}$ viewed down the (a) [1 0 0] and (b) [0 1 0] directions. (c) and (d) Corresponding views of the $P1$ structure of $Bi_7Ta_3O_{18}$ (10), with pseudosymmetry elements indicated. Bismuth atoms are darker than TaO_6 atoms, and oxygen atoms are black.

the use of independent displacement parameters resulted in slightly negative values for Ta(1), Ta(2), O(4), and O(11). The final model described below refers to the previous refinement, using two isotropic displacement parameters, one for metal and one for oxygen atoms.

The observed, calculated and difference powder neutron diffraction profiles for the final refined $P\bar{1}$ structure of $Bi_4Ta_2O_{11}$ are shown in Fig. 2. Refinement statistics for individual histograms are presented in Table 2. Final refined values for the fractional coordinates and U_{iso} values are given in Table 3. The final refined unit cell parameters were $a = 6.60890(8)$, $b = 7.65686(10)$, $c = 9.88280(13)$ Å, $\alpha = 101.3445(19)$, $\beta = 90.1829(15)$, $\gamma = 90.029(3)^\circ$, $V = 490.329(11)$ Å^3.

Bond valence sums (13) for the initial model and the final refined structure of $Bi_4Ta_2O_{11}$ are presented in Table 4. Note that those atoms in the initial model for which the bond valence sums are furthest from expected values are those closest to the $z = 1/2$ plane, where average coordinates about the inversion center were used. In this context, the initial model is chemically reasonable. Nonetheless, the refined structure clearly represents a significant improvement and therefore strongly supports the validity of the refinement.

DISCUSSION

The final refined $P\bar{1}$ structure of $Bi_4Ta_2O_{11}$ is shown in Figs. 3a and 3b, compared to the $P1$ structure of $Bi_7Ta_3O_{18}$ in Figs. 3c and d. The relationship between the two phases, as members of a homologous series of layered structures, is obvious from Fig. 3. For all types of atoms, the same connectivity and coordination environments are observed in both structures. The only significant difference is in the relationship between the distribution and orientation of TaO_6 octahedra in mixed metal atoms layers (perpendicular to c) separated by Bi-only layers. In $Bi_7Ta_3O_{18}$, this relationship (approximately) incorporates both a mirror plane and a twofold rotation axis (indicated in Figs. 3c and 3d), lending the structure pseudo-$C2/m$ symmetry in an alternative setting (10). The breaking of both symmetry elements lowers the symmetry to $P1$ rather than $P\bar{1}$. In $Bi_4Ta_2O_{11}$, Fig. 3a shows that these symmetry elements are forbidden; the twofold rotation axis by Ta distribution within the metal atom layers and the mirror plane by the rotation of TaO_6 octahedra. An inversion center is allowed and appears to hold. It should be noted, however, that the refinement of $Bi_7Ta_3O_{18}$ using powder neutron diffraction data (10) could not effectively refine the symmetry lowering from $C2/m$ to $P1$. The possibility therefore exists that with single crystal X-ray data, particularly with the benefit of anomalous scattering, a $P1$ model for the structure of $Bi_4Ta_2O_{11}$ might lead to a more satisfactory solution. At this stage it has not been possible to grow single crystals of $Bi_4Ta_2O_{11}$.

We have previously demonstrated (7) that neither $Bi_7Ta_3O_{18}$ nor $Bi_4Ta_2O_{11}$ possess unambiguous fluorite-type subcells of the type described by Zhou (9). Nonetheless, electron diffraction patterns of both phases did display some distinctly fluorite-like projections. These patterns are explained in the case of $Bi_7Ta_3O_{18}$ by describing the structure as consisting of layers of pseudo-fluorite-type which are "stepped" on the $z = 0$ planes (perpendicular to the $[1\,1\,1]_{fluorite}$ direction) (10). On these stacking fault planes, two adjacent metal layers form a primitive hexagonal (rather than an fcc) array. The same phenomenon underlies the fluorite-like projections observed for $Bi_4Ta_2O_{11}$. There is clearly no meaningful average fluorite-related subcell for the diffraction patterns of either phase, despite this relationship to a fluorite substructure in real space.

As in the case of $Bi_7Ta_3O_{18}$, the coordination environments of tantalum atoms in $Bi_4Ta_2O_{11}$ consist of regular octahedra forming columns along the [0 1 0] direction. Octahedral rotations in the order of $\sim 10^\circ$ about the [1 0 0] direction are observed. Also, as for $Bi_7Ta_3O_{18}$, the coordination environments of bismuth atoms are difficult to define; they appear to be related to the cubic (eightfold) coordination found in fluorite, distorted by the presence of TaO_6 octahedra such that Bi–O bond lengths vary between 2.0 and 3.0 Å. Setting the maximum Bi–O bond length at 2.7 Å differentiates the environments of Bi(1) and Bi(2) from those of Bi(3) and Bi(4). The former two are located on the basal planes of square pyramids, a coordination observed in $Bi_7Ta_3O_{18}$ and typical of cations with stereochemically active electron lone pairs such as Bi^{3+}, the archetype being α-PbO (14). The latter two occupy sites not observed in $Bi_7Ta_3O_{18}$, and shown in Fig. 4. These sevenfold sites are

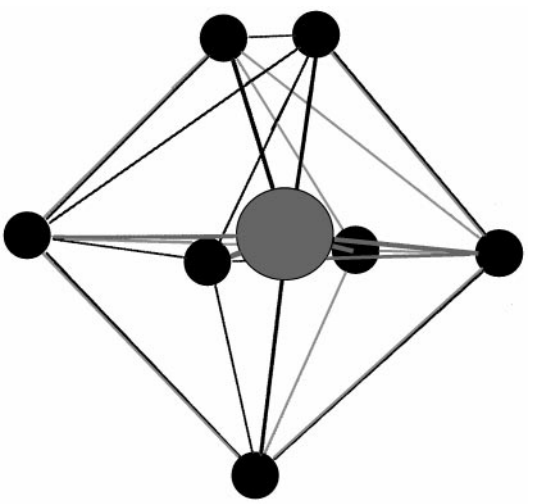

FIG. 4. The coordination environment of Bi(4). Oxygen atoms are black.

clearly oxygen-deficient variations on the eightfold cubic sites found in fluorite-type.

The two phases discussed here are the tantalum-rich members of a series of four in the Bi_2O_3–Ta_2O_5 system reported by Zhou (9) as being based on superstructures of fluorite-type δ-Bi_2O_3: I ($Bi_{15}TaO_{25}$), II (Bi_9TaO_{16}–Bi_3TaO_7), II* ($Bi_7Ta_3O_{18}$), and III ($Bi_4Ta_2O_{11}$). A fifth phase, type IV (8,15), was considered too far removed from a fluorite-type substructure to be described in the same way. In our recent reinvestigation of these phases (7) we proposed that while types I and II were clearly fluorite-related superstructure phases, types II* and III were not. This proposition has been borne out in the present study, therefore the solved structures of types II* and III cannot be used to directly elucidate the structures of types I and II. The type IV phase is thought, on the basis of a TEM study (15), to be a hybrid of the $n = 1$ and $n = 2$ Aurivillius series of phases. This model incorporates extensive perovskite units, hence the bulk of the metal atom array departs from the fluorite arrangement found in the bulk of the type II* and III structures. This means that the type II* and III structures do not directly contribute to an understanding of the type IV phase either.

CONCLUSION

The existence of these two closely related phases, neither of which have fluorite-type subcells, demonstrates that the principles on which their structures are based are more complicated than formerly proposed. It was previously thought that δ-Bi_2O_3 was the sole archetype for the type I, II, II*, and III phases in the Bi_2O_3–Ta_2O_5 system (9). The usefulness of a modulated δ-Bi_2O_3 description clearly ends with type II, subsequent (more Ta-rich) phases being better described as layered or intergrowth structures.

ACKNOWLEDGMENTS

The authors gratefully acknowledge the financial assistance of the Australian Synchrotron Research Programme and the Access to Major Research Facilities Programme in the collection of X-ray and neutron data respectively. The assistance of Dr David Cookson in the collection of synchrotron X-ray data and the assistance of Dr Ron Smith in the collection of neutron data are also greatly appreciated.

REFERENCES

1. T. Takahashi and H. Iwahara, *Mater. Res. Bull.* **13,** 1447 (1978).
2. A. W. Sleight, *Science* **208**(4446), 895 (1980).
3. G. Gattow and H. Schröder, *Z. Anorg. Allg. Chem.* **318,** 176 (1962).
4. H. A. Harwig, *Z. Anorg. Allg. Chem.* **444,** 151 (1978).
5. A. R. Allnat and P. W. M. Jacobs, *Chem. Rev.* **67, 681 (**1967).
6. A. R. Allnat and P. W. M. Jacobs, *Proc. R. Soc. London Ser.* A**260,** 350 (1961).
7. C. D. Ling, R. L. Withers, S. Schmid, and J. G. Thompson, *J. Solid State Chem.*
8. E. M. Levin and R. S. Roth, *J. Res. Natl. Bur. Stand.* **68**A [2], 197 (1964).
9. W. Zhou, *J. Solid State Chem.* **101,** 1 (1992).
10. C. D. Ling, S. Schmid, R. L. Withers, and J. G. Thompson, submitted for publication.
11. S. Hull, R. I. Smith, W. I. F. David, A. C. Hannon, J. Mayers, and R. Cywinski, *Physics* B **180** and **181,** 1000 (1992).
12. A. C. Larson and R. B. Von Dreele, "GSAS. The General Structure Analysis System." Los Alamos National Laboratory, 1991.
13. N. E. Brese and M. O'Keeffe, *Acta Crystallogr. B* **47,** 192 (1991).
14. B. G. Hyde and S. Andersson, "Inorganic Crystal Structures," p. 257. Wiley, New York; 1989.
15. W. Zhou, D. A. Jefferson, and J. M. Thomas, *Geophys. Monogr.* **43,** 113 (1989).